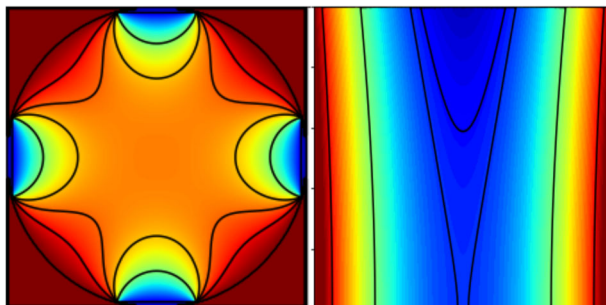Check for updates

RESEARCH ARTICLE

Analytical Solution for the Electric Field Inside Dynamically Harmonized FT-ICR Cell

Anton Lioznov,[1] Gökhan Baykut,[2] Evgeny Nikolaev[1]

[1]Skolkovo Institute of Science and Technology, Moscow, Russia
[2]Bruker Daltonik GmbH, Bremen, Germany

Abstract. Dynamically harmonized FT-ICR cell has a saddle-like hyperbolic field distribution inside when averaged over a cyclotron trajectory around the axis of the cell. Such a field distribution makes the motion along the magnetic field independent of the motion in the x,y-plane, as well as the cyclotron motion independent of the magnetron motion and prevents any disintegration of excited coherent ion clouds, which is ruining the resolution in the other types of FT-ICR cells providing by this ideal phasing of single-m/z ion clouds in the entire volume of the cell. FT-ICR instruments with such a cell show resolutions of more than ten million at m/z 1000 at relatively small magnetic fields like 7 Tesla in quadrupole detection mode, what is not reachable by any other type of modern mass spectrometers. We have found that for such ion traps, it is possible to find the analytical solution in the working volume of the trap without any averaging. The potential distribution for the almost whole volume of such a cell can be presented in the form $\phi(x, y, z) = \alpha z^2 + f_{2D}(x, y)$, where $f_{2D}(x, y)$ is the solution of 2D Poisson equation, which could be found by the method of conformal transformation. This solution is applicable in the practical case and can serve as a base for an analytical theory of signal detection using such cells and as a standard for solutions obtained by numerical simulations of the cell field.

Keywords: Fourier-transform ion cyclotron resonance, Dynamically harmonized FT ICR cell, Paracell, Conformal mapping

Introduction

The consistent leadership of the Fourier-transform ion cyclotron mass spectrometry (FT-ICR MS) in resolving power and mass precision among all existing mass spectrometry methods experienced a big leap upon introduction of the new FT-ICR cell with dynamic harmonization [1–3]. Dynamic harmonization was implemented in commercial FT-ICR mass spectrometers of (Bruker's "Solarix xR" "Solarix 2xR" and "Scimax") and in National High Magnetic Field Laboratory in the FT-ICR system with highest magnetic field of 21 Tesla [4]. Excitation and detection segments of this ICR cell consist of assemblies of electrodes which are shaped in a way that the electric field distribution in the cell is harmonic (saddle-like

hyperbolic) when averaged over a cyclotron trajectory around the axis of the cell[1].

Such a field distribution separates the ion motion along the magnetic field from the motion in x,y-plane, as well as the cyclotron motion from the magnetron motion. This protects the excited coherent ion clouds from losing their angular integrity by a so-called comet formation [5] and provides ideal phasing of single m/z ion clouds in the whole volume of the cell during detection [6] FT-ICR

Correspondence to: Evgeny Nikolaev; *e-mail:* e.nikolaev@skoltech.ru

---

[1]Here and later in the text, we are talking about averaging along axis-center cyclotron motion trajectory. This averaging coincides with averaging along the azimuthal angle. By this, we are pointing out that cyclotron frequency is much higher than axial oscillation frequency and the forth moving ions along z-axis is averaged over the cyclotron motion

instruments with dynamically harmonized cells demonstrated at relatively low magnetic fields like 7 Tesla mass resolving power over ten million at m/z 1000 in quadrupole detection mode, which was not reachable with any other type of modern mass spectrometric devices.

In [1], we have provided the theory of dynamically harmonized cell (DHC) for the case of cyclotron motion-averaged field distribution. In the past, attempts were made to develop an analytical theory of the field distribution inside the tetragonal and cylindrical FT ICR cells. Nikolaev and Gorshkov give a theory of field distribution in elongated (infinitely long) cylindrical cells by using conformal mapping [7]. Grosshans, Shields, and Marshall [8] found the equations for the field as infinite series of Bessel functions for these trap geometries through the Green's functions formalism. Although such an approach is successful, the resulting equations are hard to use in field calculation and analysis because of the presence of infinite sums.

In the present paper, we have extended the theory developed in Boldin and Nikolaev paper [1] to the case of the non-averaged field. Our working hypothesis is based on the assumption that the potential distribution in a dynamically harmonized cell can be presented in the form $\phi(x, y, z) = \alpha z^2 + f_{2D}(x, y)$, where $f_{2D}(x, y)$ is the solution for 2D Poisson equation, that can be found by the method of conformal mapping and α is a coefficient, that can be found from boundary conditions (trapping potentials). The separation of variables reduces the number of dimensions from 3 to 2 and significantly simplify the equations.

In order to verify the model, the comparison with numerical simulation was made.

The obtained potential distribution can serve as a base for an analytical theory of signal detecting using dynamically harmonized cells and as a standard for solutions obtained by numerical simulations of the cell field.

Theory

The formal statement of the problem: We need to solve the Laplace equation for the electric potential

$$\Delta_{x,y,z} \phi(x, y, z) = 0 \tag{1}$$

With the boundary conditions (Figure 1)

$$\phi|_{r=R} = \begin{cases} 0, & \theta \in \frac{2\pi}{N} n \pm \beta \frac{\pi}{N} \left(1 - \frac{z^2}{z_0^2}\right) \\ \phi_0, & \theta \in \frac{2\pi}{N} \left(n + \frac{1}{2}\right) \pm \left(\frac{\pi}{N} + \beta \frac{\pi}{N} \left(\frac{z^2}{z_0^2} - 1\right)\right) \end{cases} \tag{2}$$
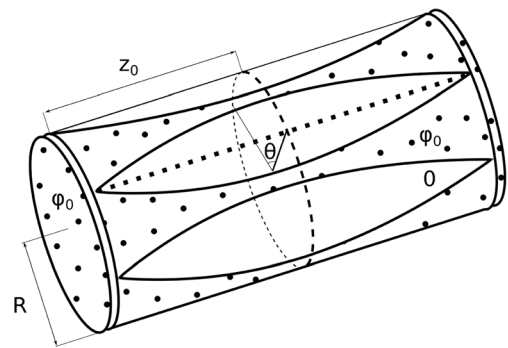
---

[2] The ratio between the width of grounded and non-grounded electrodes in the middle ($z = 0$) of the cell.
[3] Arctan2 (y, x) is the modification of arctan (y/x) with range of value $[-\pi, \pi]$.

Figure 1. The geometry of the dynamically harmonized FT-ICR cell. The "leaf" electrodes have zero potential, everything else ("inverse leaf" electrodes on the cylinder mantle and the end caps) is under voltage ϕ_0

where R is the radius of the cell, z_0 is its half-length ($z = 0$ is corresponds to the center of the cell), β is a coefficient responsible for the width[2] of grounded "leaf" electrodes, N is the total number of leaf electrodes, and $n = 0, 1, \ldots N - 1$ is the serial number of the leaf electrode. Here and below in some cases, we will write equations in polar coordinates: $r = \sqrt{x^2 + y^2}$, $\theta = \arctan2 (y, x)$[3], angle θ is measured from the center line of one of the grounded electrodes.

Reducing the Problem Dimensions from 3D to 2D

Averaging of the electric field in a dynamically harmonized cell performed in Boldin and Nikolaev paper [1] was made in the plane perpendicular to the magnetic field x, y-plane in our model. The averaging procedure does not involve the z-coordinate. From this fact, we can conclude that the field before the averaging process can be presented in the same form as the field averaged along the cyclotron motion trajectory:

$$\phi(x, y, z) = \alpha \cdot z^2 + f_{2D}(x, y) \tag{3}$$

where f_{2D} is the solution of 2D Poisson equation obtained from 3D Laplace Eq. (1):

$$\Delta_{x,y} f_{2D}(x, y) = -\Delta_z \alpha z^2 \tag{4}$$

The function f_{2D} can be presented as the sum of two other functions:

$$f_{2D}(x, y) = f(x, y) + f_{pp}(x, y) \tag{5}$$

where f_{pp} is a partial solution of the Poisson equation and f is the common solution for 2D Laplace equation. Of course, such presentation of DHC field is not valid in the whole cell volume. Very close to the electrodes, the field is not quadratic along z because each electrode has a fixed potential which does not vary along the electrode. It is equipotential (for more precise explanation, see "Evaluating the Laplacian" section and Figure 5).

From (4) $\Delta_{x,y} f_{pp} = -\Delta_z \alpha z^2 = -2\alpha$. The partial solution can be obtained in the form

$$f_{pp}(x,y) = -\frac{\alpha}{2} r^2 \qquad (6)$$

The coefficient α will be calculated later from the boundary conditions.

From (1)

$$\phi(x,y,z) = f(x,y) + \alpha z^2 - \frac{\alpha}{2} r^2 \qquad (7)$$

The $f(x,y)$ is the solution of

$$\Delta_{x,y} f(x,y) = 0 \qquad (8)$$

With boundary conditions (from (7) and (2))

$$f|_{r=R}
= \begin{cases}
-\alpha z^2 + \frac{\alpha}{2} R^2, & \theta \in \frac{2\pi}{N} n \pm \beta \frac{\pi}{N}\left(1 - \frac{z^2}{z_0^2}\right) \\
\phi_0 - \alpha z^2 + \frac{\alpha}{2} R^2, & \theta \in \frac{2\pi}{N}\left(n + \frac{1}{2}\right) \pm \left(\frac{\pi}{N} + \beta \frac{\pi}{N}\left(\frac{z^2}{z_0^2} - 1\right)\right)
\end{cases} \qquad (9)$$

Solving the 2D Laplace Equation

It is not necessary to solve the Laplace equation with so complicated boundary condition (9). If Eq. (8) can be solved with the following conditions

$$f|_{r=R} = \begin{cases} \phi_0, & \theta \in [0, \theta_0] \\ 0, & else \end{cases} \qquad (10)$$

where θ_0 is some arbitrary angle, the electric potential with the boundary condition (9) can be found using the superposition principle with the proper choice of θ_0 (it will be described more precisely at the end of the subsection—Eqs. (17)–(19)).

The common way to solve a two-dimensional electrostatic problem is the conformal mapping. The detailed description of this method can be found in [9] and in the Appendix. In the following, we describe the main idea.

Let us take a conductor, which is infinitely long in z axis. Thus, the electric field E of the conductor depends only on x and y, but not on z. The conductor in x, y-plane can be described as a curve $C = f(x,y)$ which is an equipotential. Let us represent the plane as a complex plane with $\bar{z} = x + iy$. Then $C = f(\bar{z})$. If there is an analytical complex function $w(z)$ that turns the curve into the line $\mathrm{Im}\, w(f(\bar{z})) = \mathrm{const}$, then the potential created by this conductive line can be found as $\phi(x,y) = \mathrm{Im}\, w$ (it is said, that $w(\bar{z})$ implements the conformal mapping of the plane $\bar{z}$).

Thus, the task (as shown in Figure 2, top) is to transform the curves ζ into ζ', ξ into ξ', the points A into A' and B into B', and the inside and outside areas again into inside and outside areas.
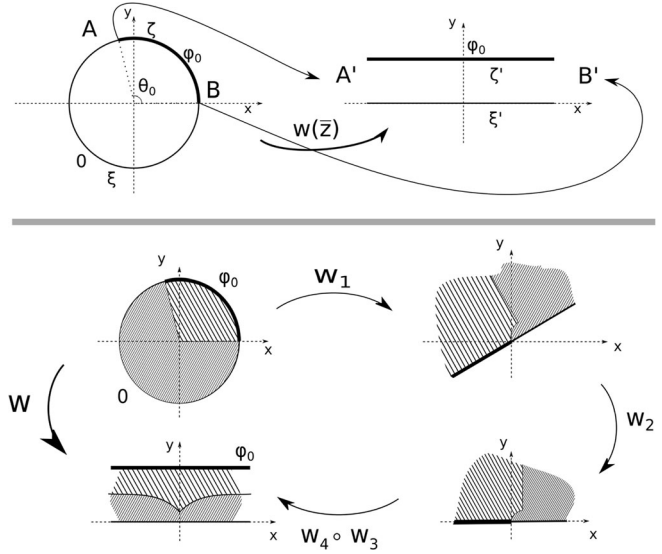

Figure 2. Top: the task, a conformal mapping $w(\bar{z})$ must transform the circle (left) to two lines (right). Bottom: The solution, the mapping of areas on the complex plane: upper-left, the initial configuration; upper-right, after applying w_1; bottom-right, after applying w_2; bottom-left, the final stage, after applying $w_4 \circ w_3$. The curve corresponded to conductor with potential ϕ_0 marked bold, the curve corresponded to grounded one marked thin

The physical interpretation of curves ζ and ξ is the cross-sections of two conductors: one with the potential ϕ_0 and the second one with the potential 0 (grounded) respectively; the points A and B are the potential leaps between the conductors.

Formally, we need to find the transformation for the curves:

$$\begin{aligned} r &= R \\ \theta &\in [0, \theta_0] \end{aligned} \quad \rightarrow \quad \mathrm{Im}\, \bar{z} = \phi_0 \qquad (11)$$

$$\begin{aligned} r &= R \\ \theta &\notin [0, \theta_0] \end{aligned} \quad \rightarrow \quad \mathrm{Im}\, \bar{z} = 0 \qquad (12)$$

And for the points:

$$R\exp(i \cdot \theta_0) \longrightarrow -\inf \qquad (13)$$

$$R\exp(i \cdot 0) \longrightarrow +\inf \qquad (14)$$

In order to perform this, we use a consecutive four-step transformation (Figure 2, bottom).

$$w = w_4 \circ w_3 \circ w_2 \circ w_1 = \frac{\phi_0}{\pi}$$
$$\cdot Ln\left[\exp(-i\theta_0/2) \cdot \frac{\bar{z} - R\exp i\theta_0}{\bar{z} - 1}\right] \qquad (15)$$

where Ln is the complex logarithm.

The functions are:

1. $w_1(\bar{z}) = (\bar{z} - R\exp i\theta_0)/(\bar{z} - 1)$ transforms the circle into the semi-plane with $w_1(1 + 0i) = 0$ and $w_1(R \exp i\theta_0) = \inf$;
2. $w_2(\bar{z}) = \bar{z} \cdot \exp(-i\theta_0/2)$ rotates the semi-plane so that the border of this plane becomes $\operatorname{Im} w = 0$;
3. $w_3(\bar{z}) = Ln(\bar{z})$ folds the semi-plane into a strip with border lines $\operatorname{Im} w = 0$ and $\operatorname{Im} w = \pi$;
4. $w_4(\bar{z}) = \phi_0/\pi \cdot \bar{z}$ normalizes the upper bound to ϕ_0.

All previous reasoning were made for the simple boundary condition (10). Before giving the solution for electric potential in this case, let us define a new function $\phi_{\theta_0,\theta_1}(x, y, \phi_0)$ as the solution for the potential with a bit more complicated boundary conditions:

$$\phi_{\theta_0,\theta_1}(x,y,\phi_0)\big|_{r=R} = \begin{cases} \phi_0, & \theta \in [\theta_0, \theta_1] \\ 0, & else \end{cases} \quad (16)$$

The solution for boundary condition (10) can now be declared as ϕ_{0,θ_0}.

Three mathematical relations are used:

1. $\operatorname{Im}(Ln(\bar{z})) = \operatorname{Arg}(\bar{z}) = \operatorname{arctan2}(y,x)^4$
2. $Ln(ab) = Ln(a) + Ln(b)$
3. $Ln(a/b) = Ln(a) - Ln(b)$

With them, from (15), the electric potential distribution can be found for simple boundary condition (10):

$$\phi_{0,\theta_0} = \frac{\phi_0}{\pi}\Big[\operatorname{arctan2}(y - R\sin\theta_0, x - R\cos\theta_0) - \frac{\theta_0}{2} \\ - \operatorname{arctan2}(y, x - R)\Big] \quad (17)$$

The next step is to solve the 2D Laplace equation with the boundary condition (16). Using the additivity principle, it can be written $\phi_{\theta_0,\theta_1} = \phi_{0,\theta_1} - \phi_{0,\theta_0}$. The solution for the electric potential with boundary condition (16) ϕ_{θ_0,θ_1} can be written as

$$\phi_{\theta_0,\theta_1}(x,y,\phi_0) \\ = \frac{\phi_0}{\pi}\Big[\operatorname{arctan2}(yR\sin\theta_1, x - R\cos\theta_1) - \frac{\theta_1}{2}\Big] - \\ - \frac{\phi_0}{\pi}\Big[\operatorname{arctan2}(y - R\sin\theta_0, x - R\cos\theta_0) - \frac{\theta_0}{2}\Big] \quad (18)$$

---

[4]Actually, we need the function image to be the segment $[0, 2\pi]$. Thus, for the whole geometric part, 2π should be added to or subtracted from the result equation, so that the resulting value at every point will be within $[0, 2\pi]$.

The final step is to find the electric potential distribution $f(x, y)$ for the boundary condition (9). Using the additivity principle once more, the $f(x, y)$ can be found from (18):

$$f(x,y) = \sum_{n=0}^{N-1}\Big[\phi_{\theta_{0,+,n},\theta_{1,+,n}}\Big(x,y,\phi_0 - az^2 + \frac{\alpha}{2}R^2\Big)\Big] + \\ = \sum_{n=0}^{N-1}\Big[\phi_{\theta_{0,-,n},\theta_{1,-,n}}\Big(x,y,-az^2 + \frac{\alpha}{2}R^2\Big)\Big] \quad (19)$$

where

$$\theta_{0,+,n} = \frac{2\pi}{N}\Big(n + \frac{1}{2}\Big) - \Big(\frac{\pi}{N} + \beta\frac{\pi}{N}\Big(\frac{z^2}{z_0^2} - 1\Big)\Big) \quad (20)$$

$$\theta_{1,+,n} = \frac{2\pi}{N}\Big(n + \frac{1}{2}\Big) + \Big(\frac{\pi}{N} + \beta\frac{\pi}{N}\Big(\frac{z^2}{z_0^2} - 1\Big)\Big) \quad (21)$$

$$\theta_{0,-,n} = \frac{2\pi}{N}n - \beta\frac{\pi}{N}\Big(1 - \frac{z^2}{z_0^2}\Big) \quad (22)$$

$$\theta_{1,-,n} = \frac{2\pi}{N}n + \beta\frac{\pi}{N}\Big(1 - \frac{z^2}{z_0^2}\Big) \quad (23)$$

Although we have assumed that $f(x, y)$ as the solution of 2D Laplace, Eq. (8) has no dependence on z-coordinate, in Eq. (19) z-coordinate is appeared as a parameter from the boundary conditions. It is showing the limitations of the theory, which will be addressed later in the text. Although the z-coordinate appeared in equation and, formally, it must be written as $f(x, y, z)$, we will still use the notation $f(x, y)$ (assuming z as a parameter), saving the connections with Eq. (8) and keeping in mind that z-coordinate has much smaller effect on the field distribution, than x or y.

Averaging over the Polar Angle

In order to find the coefficient α, we average 3D electric potential distribution over cyclotron motion (this is an equivalent of the averaging over the polar angle θ). The calculation is also useful for comparison the results with [1].

It can be proved, that the averaged over the polar angle solution of the 2D Laplace equation $\hat{f}(r)$ is independent of r (note that here, we are talking about the 2D Laplace equation, not the 2D Poisson equation and not the 3D Laplace equation). To understand the independence, note first that if $\hat{f}$ with the simple boundary condition (10) (declared as $\hat{\phi}_{0,\theta_0}(r)$) is independent of r, then the $\hat{f}$ with the actual boundary condition (9)

is independent too (because of the commutation between addition and taking the average procedures).

Let us prove that $\hat{\phi}_{0,\theta_0}(r)$ is independent of r:

$$
\begin{aligned}
\hat{\phi}_{0,\theta_0}(r) = \\
\frac{1}{2\pi}\oint d\theta \frac{\phi_0}{\pi}\arctan\frac{r\sin\theta - R\sin\theta_0}{r\cos\theta - R\cos\theta_0} - \\
-\frac{\phi_0}{\pi}\frac{1}{2\pi}\oint d\theta\frac{\theta_0}{2} \\
-\frac{\phi_0}{\pi}\frac{1}{2\pi}\oint d\theta\arctan\frac{r\sin\theta}{r\cos\theta - R}
\end{aligned}
\tag{24}
$$

Coming from the simplest to the hardest one:

- The second integral is obviously constant: it is taken from a constant function
- The third one is equal to zero because of the oddness: $r\sin\theta$ is odd, $r\cos\theta - R$ is even, a quotient of odd and even is odd, arctan is odd, so arctangent from an odd function is odd as well. An integral over a circle from the odd function gives us zero.
- The first integral is constant because of the geometric meaning of the arctan. Arctangent is an angle from x-axis to the line between origin and the point $(r\sin\theta - R\sin\theta_0, r\cos\theta - R\cos\theta_0)$. The averaging of an angle over the angle is constant.

The $\hat{f}(r) = \hat{f}(R)$ for all r can be found from (9):

$$
\hat{f} = \phi_0\left(1 - \beta\left[1 - \frac{z^2}{z_0^2}\right]\right) - \alpha z^2 + \frac{\alpha}{2}R^2
\tag{25}
$$

Return to the 3D equation

$$
\hat{\phi}(r,z) = \phi_0 - \beta\left(1 - \frac{z^2}{z_0^2}\right)\phi_0 + \frac{\alpha}{2}\left(R^2 - r^2\right)
\tag{26}
$$

Now, the α coefficient can be determined. From (7) and (26):

$$
2\alpha = \frac{\partial^2\phi}{\partial z^2} = \frac{\partial^2\hat{\phi}}{\partial z^2} = \frac{2\beta\phi_0}{z_0^2}
\tag{27}
$$

Solving the Original Equation

So, the formula for electric potential from (3), (6), (19), and (27)

$$
\begin{aligned}
\phi(r,\theta,z) = \phi_0\frac{\beta}{z_0^2}z^2 - \phi_0\frac{\beta}{2z_0^2}r^2 + \\
+ \sum_{n=0}^{N-1}\left[\phi_{\theta_{0,+,n},\theta_{1,+,n}}\left(x,y,\phi_0 - \phi_0\frac{\beta}{z_0^2}z^2 + \phi_0\frac{\beta}{2z_0^2}R^2\right)\right] + \\
+ \sum_{n=0}^{N-1}\left[\phi_{\theta_{0,-,n},\theta_{1,-,n}}\left(x,y,-\phi_0\frac{\beta}{z_0^2}z^2 + \phi_0\frac{\beta}{2z_0^2}R^2\right)\right]
\end{aligned}
\tag{28}
$$

With function (18) and angle (23).
Simplifying the whole equation, we finally get:

$$
\phi(r,\theta,z) = \frac{\beta\phi_0}{2z_0^2}\left(R^2 - r^2\right)
$$

$$
+ \frac{\phi_0}{\pi}\sum_{n=0}^{N-1}\left(\arctan\frac{y - R\sin\theta_n}{x - R\cos\theta_n}\right)\Bigg|_{\theta_n = \frac{\pi}{N}\left(2n - \beta\frac{z^2}{z_0^2} + \beta\right)}^{\theta_n = \frac{\pi}{N}\left(2n + 2 + \beta\frac{z^2}{z_0^2} - \beta\right)}
\tag{29}
$$

Again, here, ϕ is the electric potential inside the trap, x, y, and z are the Cartesian coordinates and r, θ, and z are the corresponding cylindrical coordinates, β is an arbitrary coefficient of ground electrodes' width, ϕ_0 is the potential of non-grounded electrode, R, z_0 are geometric parameters of the trap, N is the number of the

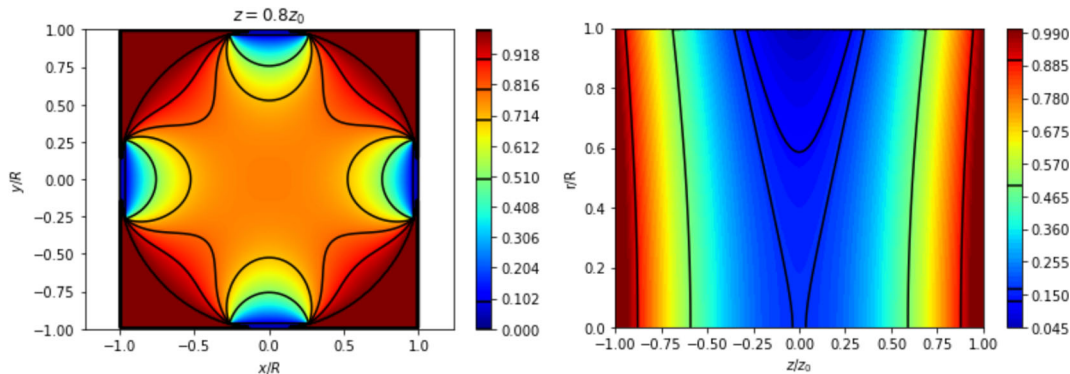**Figure 3.** The distribution of potential at $z = 0.8z_0$, $z_0 = 60$mm, $R = 30$mm, $\beta = 0.95$, $N = 4$ (left) and the averaged over polar angle distribution for the same cell (right)
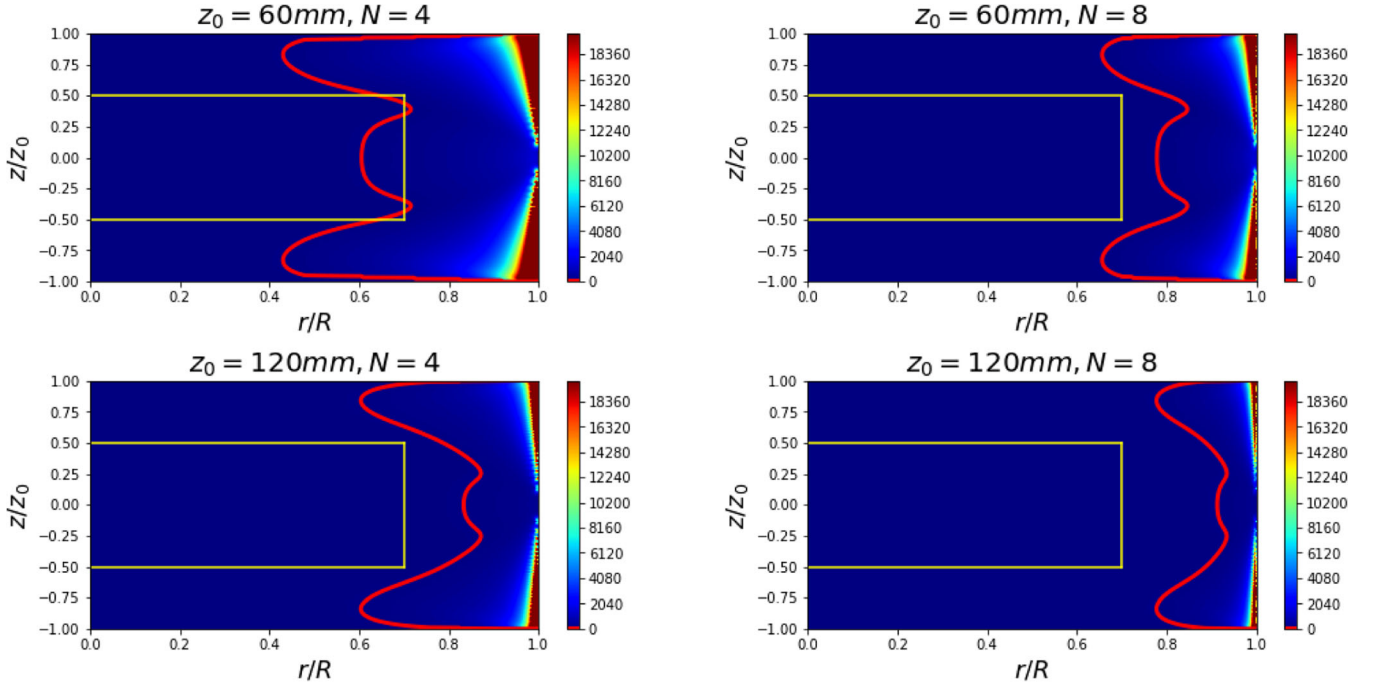
Figure 4. Mean deviation from zero of the Laplacian (in V/m^2), averaged over angle. $\beta = 0.95$, $R = 30$mm, $\varphi_0 = 1V$. For more clear view of low values we transform values bigger than 2×10^4 to the log scale. Red line is showing the border where Laplacian is equal to 10^2. The area inside the yellow lines is the working area. Laplacian become closer to zero with increasing of z_0 and N

grounded electrodes (Figure 1), vertical line stands for subtraction of two arctangents.

For averaged electric potential we get from (26) and (27):

$$\hat{\phi}(r,z) = \phi_0 - \frac{2\beta\left(1-\frac{z^2}{z_0^2}\right)}{2}\phi_0 + \frac{\beta\left(1-\frac{r^2}{R^2}\right)R^2}{2}\frac{R^2}{z_0^2}\phi_0 \quad (30)$$

This equation is the same as in [1] with $\alpha_0 = \beta \cdot \pi/N$.

Figure 3 shows the electric potential distribution at particular $z = 0.8z_0$ (left) and the averaged potential distribution (right) for the typical cell with following parameters: $N = 4$, $\beta = 0.95$, $R = 30$mm, $z_0 = 60$mm.

Evaluating the Laplacian

The final solution (29) must be checked if it is satisfying the Laplace Eq. (1).

The second derivatives over x and y: the first term in (29) gives $\partial^2 \phi/\partial x^2 = \partial^2 \phi/\partial x^2 = -\frac{\beta\phi_0}{z_0^2}$; the second derivative of the second term (with summation over n) is zero as the strict solution of 2D Laplace equation. The second derivative over z is obtained by the direct calculation.

The full Laplacian is shown below

$$\Delta\phi(x,y,z) = -\frac{2\beta\phi_0}{z_0^2} +$$

$$+\frac{\phi_0}{\pi}\sum_{n=0}^{N-1}\left[\frac{(R^2-r^2)s\beta\frac{2\mu}{Nz_0^2}}{2\left(R^2+r^2-2R(x\cos\theta_n+y\sin\theta_n)\right)} - \frac{2R(R^2-r^2)\left(\beta\frac{2z\pi}{Nz_0^2}\right)^2(x\sin\theta_n-y\cos\theta_n)}{2\left(R^2+r^2-2R(x\cos\theta_n+y\sin\theta_n)\right)^2}\right]$$

$$\left.\theta_n = \frac{\pi}{N}\left(2n+2+\beta\frac{z^2}{Z_0^2}-\beta\right), s = +1\right.$$
$$\left.\theta_n = c\pi N\left(2n-\beta\frac{z^2}{Z_0^2}+\beta\right), s = -1\right.$$

$$(31)$$

The Laplacian is not equal to zero in the whole space. Its averaged over angle deviation from 0^5 is shown in Figure 4 for different N and z_0. The area inside the yellow lines is the working area of the trap. Its boundaries are the following: $z = \pm 0.5z_0$, $r = 0.7R$. The boundary of the working region of the trap corresponds to the region of high homogeneity of the magnetic field (usually a cylindrical region of 6 cm long and 6 cm in diameter). In radial directions, it is limited by the demands of avoiding the odd harmonics in the FT-ICR signal. The red line is the border of the region where the Laplacian is equal to 10^2V/m^2.

$^5(1/2\pi)\oint d\theta \cdot |\Delta\phi(r,z,\theta)|$

Table 1. Maximum Value of the Laplacian in V/m^2 in the Working Areas for Different N and z_0. $R = 30mm$, $\beta = 0.95$, $\phi_0 = 1V$

N (mm) z_0	4	8
60	347	62
120	87	16

The absolute value and the sign of the Laplacian can be different depending on a particular z and θ, but is always close to zero in the larger part of the working volume and become significant only closer to the working area borders. Moreover, as it is shown in the figure, the deviation becomes closer to zero with increasing of z_0/R and N.

The maximum value of the Laplacian for each case inside the boundaries was also calculated. The maximum value of the Laplacian depends on z_0 and N as shown in Table 1.

In close proximity to the electrodes, the potential should not follow the z^2-law, because of the influence of the nearest electrode, which is equipotential. In common case, keeping x, y constant, by changing z-coordinate, the potential would have a leap from ϕ_0 to zero and back again: when $z = -z_0$, the
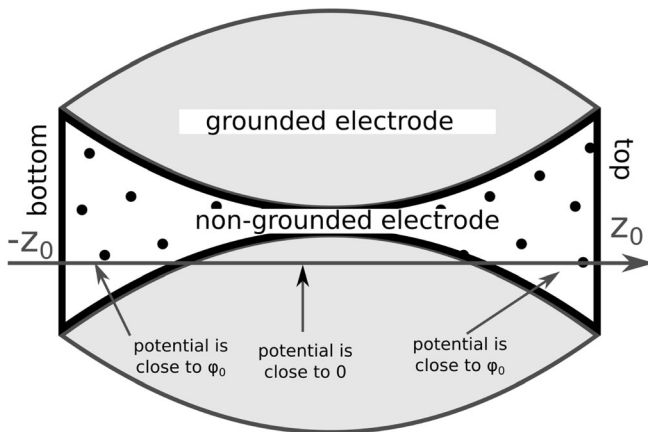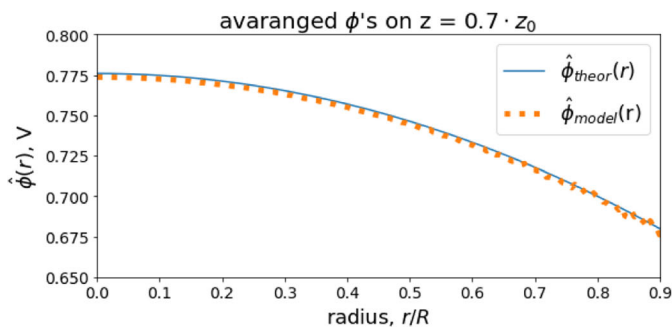

Figure 5. Changes of the potential inside the cell near the electrodes with fixed x and y

nearest electrode has potential ϕ_0, going upward the nearest electrode changes to the grounded one, and continue going upward the nearest electrode changes ones more to the electrode $\phi = \phi_0$ (see Figure 5). That is why the coordinate separation becomes invalid. When moving away from the cell electrodes, the influence of the equipotential electrode decreases, as shown in Figure 4 and Table 1.

The physical meaning of the value of the Laplacian at a point is simple—it is just the value of imaginary space charge at this point as follows from the Poisson equation:

$$\Delta\phi = \frac{\rho}{\epsilon_0}; \qquad \epsilon_0 \sim 9 \cdot 10^{-12} F \cdot m^{-1} \qquad (32)$$

Thus, the physical meaning of the non-equality to zero of the Laplacian could be attributed to the imaginary charges. If this density is much less than the density of real ions presented in the cell, then the approximation is good.

Inside the working volume, the biggest value of the Laplacian is $\sim 100 V/m^2$. From (32), it can be calculated that such a value corresponds to less than ten ions in mm^3. Typical ion cloud has the volume $V \sim 10^2 - 10^3 mm^3$ [10]. For ion number $\sim 10^5$, there are more than 100 ions in $1 mm^3$. Thus, even with the biggest Laplacian in the whole area, the number of imaginary ions are much less than the number of real ions. The simulations show that this range is more than enough for a good approximation as it will be shown in the next section.

Comparison with Computer Simulation Results

It is interesting to compare the analytically calculated field with a simulated one. The electric field distribution was determined using the finite difference method for the Laplace equation in the Cartesian coordinates by using SIMION 8.1. The data analysis and comparison was carried out by Python 3.6. Two types of comparisons were performed: the comparison between the averaged
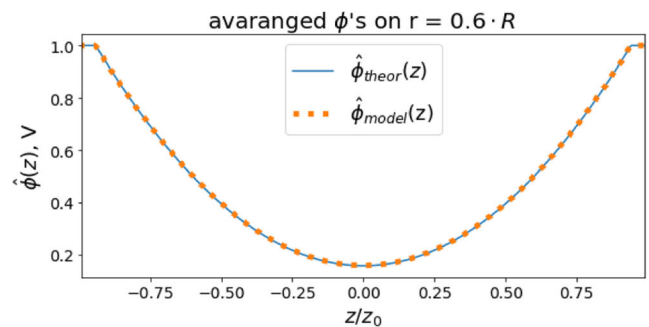

Figure 6. The comparison between the averaged over the polar angle potentials, simulated and theoretical. The left part of the figure shows the r-dependence with fixed z, the right part shows the z-dependence with fixed r
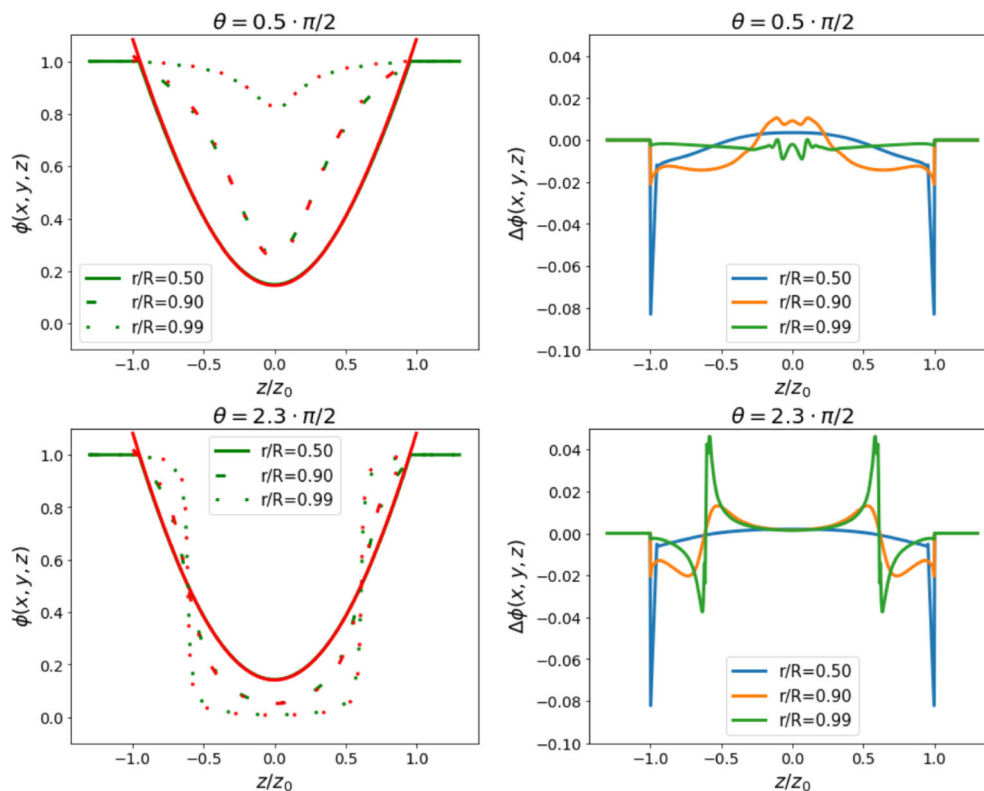
Figure 7. Left, comparison of the results for φ obtained by the theory (green lines) and obtained by the simulation (red lines). They coinside for r/R = 0.5 . In each figures, different radii are marked by solid, dash-dotted, and dotted lines. Right, the difference between the results of the simulation and the theory. Each of two figures in left and right rows stands for one fixed angle, which is shown in the title of a figure. $R = 30$mm, $z_0 = 60$mm, $N = 4$, $\beta = 0.95$

field (in order to double-check the simulation) and the comparison between the unaveraged field.

Comparison of Averaged Fields

The comparison between theory ϕ_{theor} and simulation ϕ_{model} after averaging over the polar angle is shown in Figure 6. In this example, the following parameters were taken: $R = 30$mm, $z_0 = 60$mm, $N = 4$, and $\beta = 0.95$; number of steps of partitioning by axes x, y, and z: 330, 330, and $2 \cdot 330$. The results match up with an accuracy of 10^{-3}.

Comparison of Unaveraged Fields

Figure 7 shows the comparison between theory and simulation in the non-averaged case. The left part of the figure shows the $\phi(z)$ dependence for several θ and r in both theoretical and simulated case. The right part of the figure shows the difference between the approaches. The upper angle $(0.5 \cdot \pi/2)$ is the angle of the plane cutting the cell between grounded leaf electrodes. The lower angle $(2.3 \cdot \pi/2)$ is an example of the general case.

In a narrow region at the junction of two electrodes, a strong disagreement of up to 20% is observed between the simulation

and the theory. But fortunately, this mismatching is limited only to this very narrow region.

Conclusion

The analytical solution for the potential distribution in the working volume of dynamically harmonized FT-ICR cell was found. Averaged field over the polar angle was calculated and it was proved that the field coincides with the averaged field obtained in the paper of Boldin and Nikolaev [1].

Distributions of two values — the Laplacian of the potential and the difference between the analytically found potential and its simulation using SIMION-8.1 — were calculated to verify the model. Both values should be equal to zero in the whole volume of the cell if the hypothesis of the field structure we are using is valid (Eq. (3)), though it is not exactly fulfilled.

The difference from zero for both distributions become significant at close proximity of the electrodes. It turns out because of non-constant second derivative over z, which was assumed as a base during construction of equations. It happened because of contribution of the nearest electrode, which is equipotential. The border between two electrodes lies at different angles depending on z. Thus the potential

depending on z (with fixed x and y) approximately takes only two constant values (ϕ_0 and 0) with the leaps between.

Both distributions—Laplacian and difference between the theory and the simulation—are becoming closer to zero inside the working area—$z \in \pm 0.5z_0$, $r < 0.7R$. So, in the working area, the theoretical potential satisfies the Laplace equation and it is in the good agreement with the simulation. And the distributions become even closer to zero with increasing the number of electrodes N and with elongation of cell—increase of z_0/R. Therefore, we conclude that the found equation can be applied for all practical cases and serve to calculate the electric field and the ion trajectories inside the cell. With the help of the reciprocity principle the solution will help to calculate the signal induced by ions moving in FT-ICR cells.

Further research is required to analyze the influence of the non-ideality of the electrode shapes and the electrode misalignments.

Acknowledgements

Appendix. About conformal mapping

Conformal mapping is a method from the theory of functions of a complex variable, which can be used for finding strict solutions of the electric potential distribution in case of a flat electric field (when E depends only on x and y, but not on z).

From [9]:

In the empty space, the electric field satisfies the equations $\mathrm{rot}E = 0$, $\mathrm{div}E = 0$. We can introduce both scalar and vector potentials for the same electric field: $E = -\mathrm{grad}\,\phi = \mathrm{rot}\,A$. Because the field is considered to be flat, the potential A can be chosen perpendicular to the plane.

Then

$$E_x = -\frac{\partial \phi}{\partial x} = \frac{\partial A}{\partial y}; \quad E_y = -\frac{\partial \phi}{\partial y} = -\frac{\partial A}{\partial x} \qquad (33)$$

This relations between A and ϕ can be also found in the theory of functions of a complex variable—the Cauchy-Riemann equations, the complex expression

$$w = \phi - iA \qquad (34)$$

Is analytical function from the complex argument $z = x + iy$.

From mathematical point of view, $w = w(z)$ implements a conformal mapping for the variable z to the plane w. If there is a conductor with x, y-plane cross-section C, and we can find some analytical function $w(x + iy)$, when in new geometry potential distribution can be found (ex: if we transform the counter C into the line $w = \phi_0$), Re w will be the potential distribution (or Im w for case of $w = i\phi_0$).

References

1. Boldin, I.A., Nikolaev, E.N.: Fourier transform ion cyclotron resonance cell with dynamic harmonization of the electric field in the whole volume by shaping of the excitation and detection electrode assembly. Rapid Commun. Mass Spectrom. **25**(1), 122–126 (2010)
2. Nikolaev, E.N., Boldin, I.A., Jertz, R., Baykut, G.: Initial experimental characterization of a new ultra-high resolution FTICR cell with dynamic harmonization. J. Am. Soc. Mass Spectrom. **22**, 1125–1133 (2011)
3. Nikolaev, E.N., Vladimirov, G., Boldin, I.A.: Influences of non-neutral plasma effects on analytical characteristics of the top instruments in mass spectrometry for biological research. AIP Conf. Proc. **1521**(1), 281–290 (2013)
4. Hendrickson, C.L., Quinn, J.P., Kaiser, N.K., Smith, D.F., Blakney, G.T., Chen, T., Marshall, A.G., Weisbrod, C.R., Beu, S.C.: 21 tesla Fourier transform ion cyclotron resonance mass spectrometer: a national resource for ultrahigh resolution mass analysis. J. Am. Soc. Mass Spectrom. **26**, 1626–1632 (2015)
5. Nikolaev, E.N., Heeren, R.M.A., Popov, M., Alexander, A.V.P., Chingin, K.S.: Realistic modeling of ion cloud motion in a FOURIER transform ion cyclotron resonance cell by use of a particle-in-cell approach. Rapid Commun. Mass Spectrom. **21**(22), 3527–3546 (2007)
6. Nikolaev, E.N.: Some notes about ft icr mass spectrometry. Int. J. Mass Spectrom. **377**, 421–431 (2015) Special Issue: MS 1960 to Now
7. Nikolaev, E., Gorshkov, M.: Dynamics of ion motion in an elongated cylindrical cell of an ICR spectrometer and the shape of the signal registered. Int. J. Mass Spectrom. Ion Process. **64**(2), 115–125 (1985)
8. Grosshans, P.B., Shields, P.J., Marshall, A.G.: Comprehensive theory of the Fourier transform ion cyclotron resonance signal for all ion trap geometries. J. Chem. Phys. **94**(8), 5341–5352 (1991)
9. Landau, L., Lifshits, E., Lifshits, E., Pitaevskii, L.: Electrodynamics of continuous media: Pergamon international library of science, technology, engineering, and social studies. In: Pergamon (1984)
10. Vladimirov, G., Hendrickson, C.L., Blakney, G.T., Marshall, A.G., Heeren, R.M.A., Nikolaev, E.N.: Fourier transform ion cyclotron resonance mass resolution and dynamic range limits calculated by computer modeling of ion cloud motion. J. Am. Soc. Mass Spectrom. **23**, 375–384 (2012)